33RD INTERNATIONAL COSMIC RAY CONFERENCE, RIO DE JANEIRO 2013
THE ASTROPARTICLE PHYSICS CONFERENCE

Probing the radio emission from cosmic-ray-induced air showers by polarization measurements

TIM HUEGE[1] FOR THE PIERRE AUGER COLLABORATION[2]

[1]*IKP, Karlsruhe Institute of Technology (KIT), Postfach 3640, 76021 Karlsruhe, Germany*
[2]*Full author list: http://www.auger.org/archive/authors_2013_05.html*

auger_spokespersons@fnal.gov

Abstract: The emission of radio waves from air showers induced by cosmic rays has been attributed to the so-called geomagnetic emission process. At frequencies around 50 MHz this process leads to coherent radiation which can be observed with rather simple setups. The direction of the electric field vector induced by this emission process depends only on the local magnetic field vector and on the arrival direction of the cosmic ray. We report on measurements of the electric field vector where, in addition to this geomagnetic component, another component has been observed which cannot be described by the geomagnetic emission process. This other electric field component has a radial dependence with respect to the shower axis in agreement with predictions made by Askaryan using a charge-excess model. Our results are compared to calculations based on models that include the radiation mechanism induced by the charge-excess process.

Keywords: Pierre Auger Observatory, AERA, ultra-high energy cosmic rays, extensive air showers, radio detection, Askaryan effect

1 Introduction

In the last decade, radio detection of cosmic ray air showers has been revived through the use of powerful digital signal processing techniques. The LOPES [1] and CODALEMA [2] experiments in particular have driven these modern developments. However, these "first-generation" modern experiments only covered areas of < 0.1 km^2 and thus only had a reach in energy of up to $\approx 10^{18}$ eV. The Auger Engineering Radio Array (AERA) [3] situated within the Pierre Auger Observatory has recently been enlarged to an area of ≈ 6 km^2 covered by a total of 124 radio detector stations (RDSs) [4]. Thereby, AERA strives to pave the way for the application of radio detection at ultra-high energies.

It has been known since the experiments in the 1960s [5] and confirmed by modern experiments [1, 2] that radio emission from air showers is strongly correlated with the local geomagnetic field. The emission must thus be dominated by a geomagnetic effect, describable by time-varying transverse currents as originally derived by Kahn & Lerche [6]. However, even before Kahn & Lerche, Askaryan [7, 8] predicted that there should be an emission component related to the time-variation of the negative net charge excess in air showers, and early experiments found evidence that there is indeed a sub-dominant non-geomagnetic contribution to the radio signal [9].

These two predicted emission contributions have distinct polarization characteristics, which are imprinted on the radio signal measured at ground. The geomagnetic emission leads to linearly polarized signals, the electric field vector always being aligned with the Lorentz force. More precisely, the electric field vector points in the direction defined by $(-\vec{v}\times\vec{B})$, where $\vec{v}$ denotes the shower axis and $\vec{B}$ refers to the local geomagnetic field. In contrast, the Askaryan emission is linearly polarized with an electric field vector aligned radially with respect to the shower axis — in other words, the electric field vector orientation varies with the position of the observer. As we will show in the following, the well-calibrated dual-polarized AERA RDSs allow us to exploit polarization characteristics to identify such a radially polarized signal contribution imprinted on the dominating geomagnetic radiation.

2 Polarization measurements

In this section, we describe our detector setup and detail two independent methods to quantify the deviation from pure geomagnetic radiation measured with AERA.

2.1 AERA data

The analysis presented here rests on data which have been acquired in radio-self-triggered mode with the first 24 AERA RDSs [3] in the period from April to July 2011. At that time, the local geomagnetic field had a strength of 24μT, an inclination of -36.6° and a declination of 2.7°. The antennas used were dual-polarized logarithmic periodic dipole antennas with an effective bandwidth from 30–78 MHz. After applying a cut for zenith angles $\leq 55°$ and applying appropriate quality cuts for the Auger surface detector (SD) array, a total of 17 events coincident between the RDSs and the SD array have been found. We rely on the SD reconstruction of energy, arrival direction and core position, which are used as input for the analysis. The quoted 17 events have a detected signal in a varying number of RDSs; each of the RDSs with a detected signal contributes a data point to the following analyses.

2.2 Polarization angle analysis

In the first analysis (see also [10]), we determine the polarization angle ϕ_p for the radio pulse detected in a given RDS. Within our offline analysis software [11] we reconstruct the three-dimensional electric field vector represented in a cartesian coordinate system defined by (x,y,z) = (geographic east, geographic north, vertical up). The relative strength of the electric field components E_x and E_y,

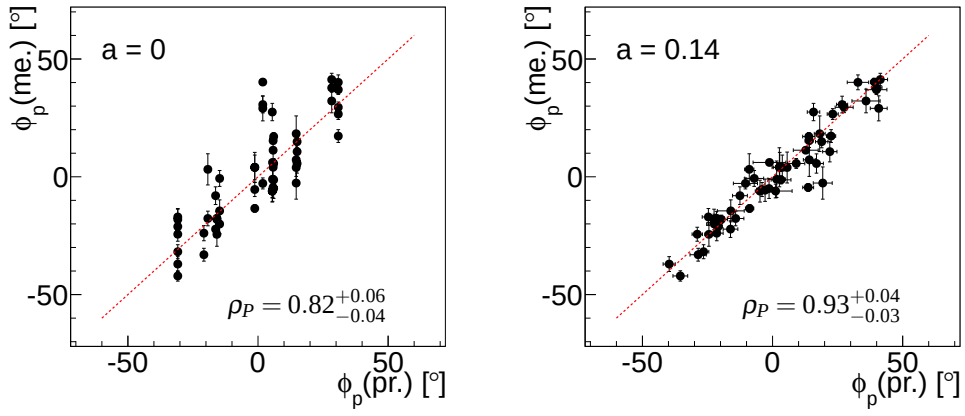

Fig. 1: Comparison of the polarization angle measured by AERA with the angle expected for pure geomagnetic radiation (left) and for a superposition of geomagnetic radiation and a contribution with radially aligned electric field vectors of a relative magnitude of 14% (right). The level of agreement is quantified with Pearson correlation coefficients and their 95% confidence levels.

representing the projection of the electric field vector to the horizontal plane, are quantified in this analysis via the use of Stokes parameters Q and U. The measured polarization angle is then given by:

$$\phi_p = \tan^{-1}\left(\frac{E_y}{E_x}\right) = \frac{1}{2}\tan^{-1}\left(\frac{U}{Q}\right). \qquad (1)$$

In the left panel of Figure 1, we compare the measured polarization angle $\phi_p(\mathrm{me.})$ with the polarization angle $\phi_p(\mathrm{pr.})$ predicted for pure geomagnetic emission with linear polarization and electric field vectors aligned according to $(-\vec{v}\times\vec{B})$. A clear correlation is visible, as expected for emission dominated by geomagnetic radiation. However, there is significant spread resulting in a $\chi^2/\mathrm{ndf.} = 27$.

In contrast, we can adopt a model for the polarization angles which corresponds to a superposition of the geomagnetic $(-\vec{v}\times\vec{B})$ contribution and a secondary linearly polarized contribution with electric field vectors oriented radially with respect to the shower axis. In this model, the parameter a denotes the relative strength of the radial contribution (E_r) with respect to the geomagnetic emission (E_g), where the latter is normalized by the sine of the angle α between the geomagnetic field and the shower axis:

$$a = \frac{|E_\mathrm{r}|}{|E_\mathrm{g}|/\sin\alpha} \qquad (2)$$

A scan has been performed to find the value of a which gives the best agreement with the totality of measured events, the result of which is $a = 0.14 \pm 0.02$. The resulting improvement is illustrated in the right panel of Figure 1; the $\chi^2/\mathrm{ndf.}$ drops to a value of 2. It is noteworthy that this value of a is in agreement with the results of [9], reporting a non-geomagnetic emission component with a strength of $14 \pm 6\%$, although it should be kept in mind that these measurements were made at a frequency of 22 MHz and at a different altitude. A detailed look at the individual events (not presented here) reveals that the value of a determined for individual events exhibits scatter at a level not compatible with a constant value of a. This additional spread has been incorporated in the scan for the mean $a = 0.14$. Future studies with a larger data set will test a potential dependence of a on air shower parameters such as zenith angle or depth of shower maximum.

2.3 R-parameter analysis

In the second analysis (see also [12]), we calculate the so-called R-parameter. To determine R, the reconstructed electric field vector is projected to the horizontal plane, and is then represented as the components along the axes ξ and η, where ξ is aligned in the direction of $(\vec{v}\times\vec{B})$ projected on the horizontal plane, and η is 90° ahead of that. In this choice of coordinate system, any electric field due to geomagnetic radiation is oriented along ξ, so any contribution along η is not of geomagnetic origin. To quantify the contributions of the electric field along ξ and η, a Hilbert-envelope is performed on the bandwidth-limited time-trace, and then a sliding window is used to find the maximum power of an integral over 25 consecutive samples (10.0 μs). The R-parameter is then defined as

$$R(\psi) \equiv \frac{2\,\mathrm{Re}(\mathscr{E}_\xi \mathscr{E}_\eta^*)}{(|\mathscr{E}_\xi|^2 + |\mathscr{E}_\eta|^2)}, \qquad (3)$$

where the $\mathscr{E}_i$ denote the η and ξ components of the complex-valued integrated Hilbert-envelope of the electric field vector and ψ denotes the observer-angle, i.e., the angle in the horizontal plane by which a given antenna is offset from the axis ξ. (For $\psi = 0$, the antenna is located in the direction defined by $\vec{v}\times\vec{B}$ with respect to the shower axis.) $R(\psi)$ thus quantifies deviations from pure geomagnetic emission polarization as a function of observer angle. The resulting distribution of R-values for the AERA data is shown in Figure 2. This R-distribution is clearly not compatible with $R \equiv 0$, which would correspond to pure geomagnetic radiation. A sinusoidal pattern appears to be visible, indicating that for particular ranges of observer angles, a significant contribution along the η axis is present.

3 Model comparison

Having shown that the cosmic ray radio emission measured with AERA cannot be explained by pure geomagnetic radiation, we compare the measured R-parameters with those derived from simulations performed with various available models. The input parameters for the event simulations are derived from the Auger SD reconstruction and comprise the particle energy, the core position, and the ar-

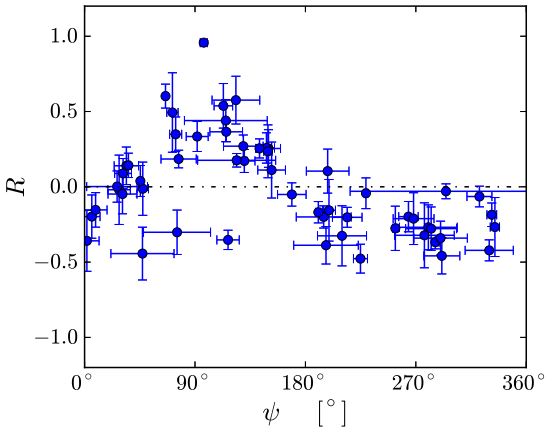

Fig. 2: *R*-parameter measured by AERA as a function of antenna observer angle ψ (see text). A horizontal line with $R \equiv 0$ is expected for pure geomagnetic radiation.

rival direction. To take into account the SD reconstruction uncertainties, each of the 17 air showers was simulated 25 times, varying all input parameters within their respective uncertainties and properly taking parameter correlations into account. The simulated electric field vectors were propagated through a detailed detector simulation taking into account the effects of the logarithmic-periodic dipole antennas, the analog electronics and the digitization. Those simulations were then reconstructed in the same way as the measured data.

In Figure 3, a direct comparison of the *R*-values predicted by the simulations and the measured *R*-values is shown. The measured and simulated *R*-values are clearly correlated, as indicated by the respective Pearson correlation coefficients (a value of 1 signifies full correlation, 0 means uncorrelated data, and -1 signifies full anti-correlation). All of these calculations include the Askaryan charge-excess contribution either explicitly (macroscopic approaches) or implicitly (microscopic approaches). A realistic refractive index of the atmosphere is incorporated for CoREAS [13], REAS [14], EVA [15] and ZHAireS [16], whereas SELFAS [17] and MGMR [18] used a refractive index of unity. In some calculations, the charge-excess contribution can be switched off. This should result in a value of $R \equiv 0$ irrespective of observer angle ψ and is confirmed by the simulation results shown in Figure 4. Without the charge-excess contribution, there is a clear disagreement between the measurements and simulations as indicated by Pearson correlation coefficients compatible with 0. This indicates that the charge-excess contribution is necessary for a proper description of the AERA data.

None of the calculations, however, can describe the measurements completely consistently, and the differences between calculations with respect to the agreement of measured and simulated *R*-parameters are relatively small.

4 Conclusion

We have shown with two different analyses that the AERA data, while dominated by linearly polarized geomagnetic emission with electric field vectors oriented along $(-\vec{v} \times \vec{B})$, exhibit a systematic deviation in the polarization of the measured signal. This deviation is consistent with a linearly polarized emission contribution with a radially aligned electric field vector. Previously, a systematic shift of the core position reconstructed on the basis of CODALEMA radio data had also indicated the presence of such a contribution with radially oriented electric field vectors [19]. The Askaryan charge-excess emission exhibits this particular polarization pattern, and a comparison of AERA data with simulations demonstrates that calculations including the Askaryan effect can reasonably describe the AERA measurements, while calculations without the Askaryan effect can clearly not. Remaining discrepancies between the modeled and measured polarization characteristics are not yet fully understood and need to be studied in further detail. Such polarization measurements can be used as a tool to test models, ideally in conjunction with other methods such as the comparison of absolute predicted amplitudes and lateral distribution functions.

References

[1] H. Falcke, W. D. Apel, A. F. Badea, et al., Nature **435** (2005) 313.

[2] D. Ardouin, A. Bellétoile, D. Charrier, et al., Astropart. Phys. **26** (2006) 341.

[3] S. Fliescher, for the Pierre Auger Collaboration, Nucl. Instrum. Meth. A **662** (2012) S124.

[4] F.G. Schröder, for the Pierre Auger Collaboration, paper 899, these proceedings.

[5] H. R. Allan, Element. Part. and Cos. Ray Phys. **10** (1971) 171.

[6] F. D. Kahn and I. Lerche, Proc. Roy. Soc. **A-289** (1966) 206.

[7] G. A. Askaryan, Soviet Phys. JETP **14** (1962) 441.

[8] G. A. Askaryan, Soviet Phys. JETP **21** (1965) 658.

[9] J. R. Prescott, J. H. Hough, and J. K. Pidcock, Nature Phys. Science **233** (1971) 109.

[10] H. Schoorlemmer, for the Pierre Auger Collaboration, Nucl. Instrum. Meth. A **662** (2012) S134.

[11] The Pierre Auger Collaboration, Nucl. Instrum. Meth. A **635** (2011) 92.

[12] D. Fraenkel, for the Pierre Auger Collaboration, J. Phys.: Conf. Ser. **409** (2013) 012073.

[13] T. Huege, M. Ludwig, and C. W. James. AIP Conf. Proc. **1535** (2013), 128.

[14] M. Ludwig and T. Huege, Astropart. Phys. **34** (2011) 438.

[15] K. Werner, K. D. de Vries, and O. Scholten, Astropart. Phys. **37** (2012) 5.

[16] J. Alvarez-Muñiz, W.R Carvalho Jr., and E. Zas, Astropart. Phys. **35** (2012) 325.

[17] V. Marin and B. Revenu, Astropart. Phys. **35** (2012) 733.

[18] K. D. de Vries, A. M. van den Berg, O. Scholten, and K. Werner, Astropart. Phys. **34** (2010) 267.

[19] V. Marin, for the CODALEMA Collaboration, Proc. 32nd ICRC, Beijing, China **1** (2011) 291.

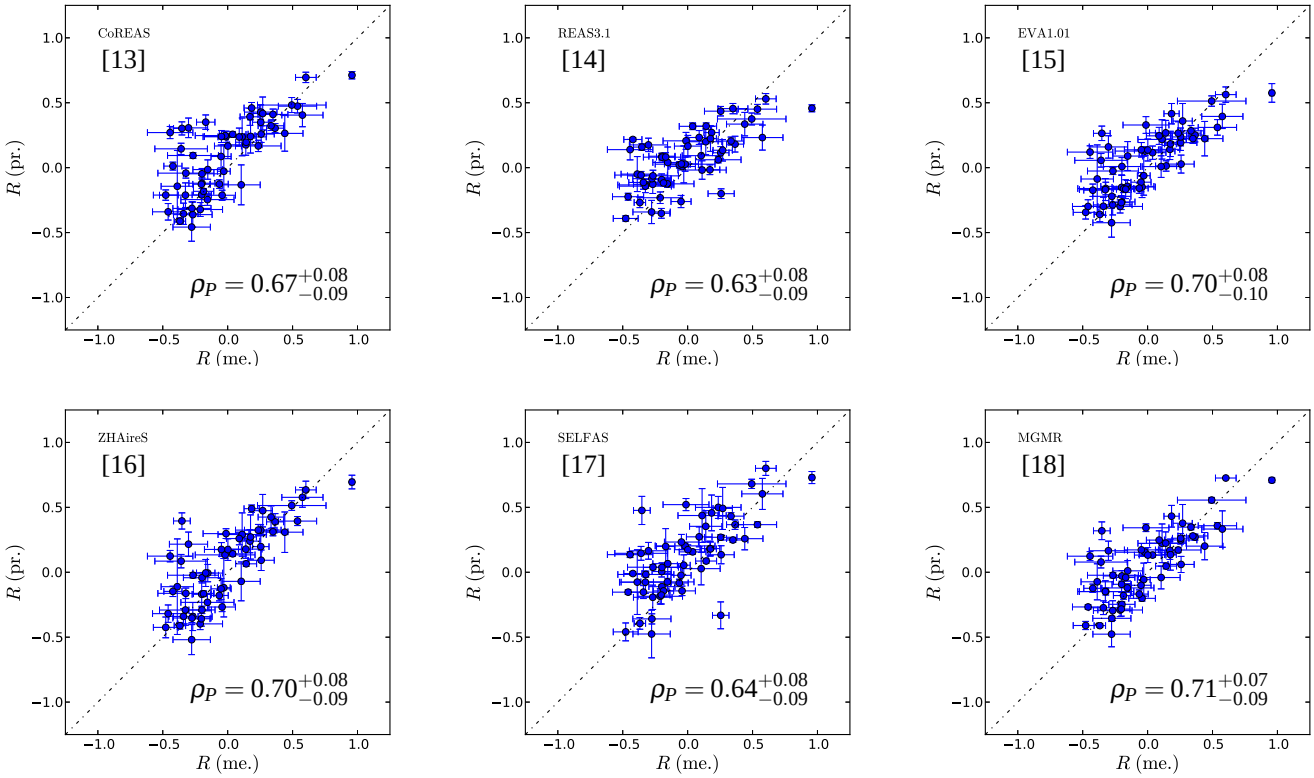

Fig. 3: Comparison of the *R*-parameters measured by AERA with six models for radio emission from extensive air showers. These calculations include the Askaryan charge-excess emission mechanism. The Pearson correlation coefficients and their 95% confidence levels quantify the level of agreement between simulation and data.

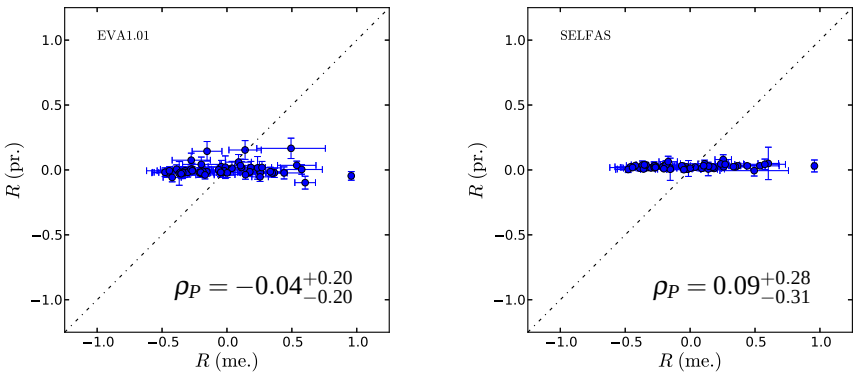

Fig. 4: Comparison of the *R*-parameters measured by AERA with two models in which the Askaryan charge-excess emission mechanism has been deactivated.